Research Square

Preprints are preliminary reports that have not undergone peer review.
They should not be considered conclusive, used to inform clinical practice,
or referenced by the media as validated information.

Functionalization of Unbleached Bambusa vulgaris Schrad. ex J.C. Wendl. Handsheets with Lignocellulose Nanofibers and Chitosan/Titanium Dioxide Surface Coating

Michaela Germaine Macalinao

mgmacalinao05@gmail.com

University of the Philippines Los Baños

Jeanette Grande-Flores

University of the Philippines Los Baños

Jessica Villanueva-Peyraube

University of the Philippines Los Baños

Ronniel Manalo

University of the Philippines Los Baños

Research Article

Keywords: bamboo, Bambusa vulgaris, hydrophobic paper, chitosan, titanium dioxide, lignocellulosic nanofibers

Posted Date: November 4th, 2025

DOI: https://doi.org/10.21203/rs.3.rs-7956019/v1

License: This work is licensed under a Creative Commons Attribution 4.0 International License.
Read Full License

Additional Declarations: No competing interests reported.

Abstract

The bamboo species *Bambusa vulgaris* Schrad. ex J.C. Wendl. is a promising fiber source in pulp and papermaking due to its rapid growth, high cellulose content, and natural abundance. This study examined the effects of handsheet functionalization with lignocellulosic nanofiber (LCNF) at 0, 10, and 15 wt%, combined with chitosan/nano-titanium dioxide (CTS/NT) surface modification on the chemical, physical, morphological, and barrier properties of bamboo-based handsheets. Unbleached kraft pulp was produced from *B. vulgaris*, with LCNF obtained through mechanical grinding. The CTS/NT coating suspension was formulated using chitosan in acetic acid, glycerol, and nano-TiO_2 dispersed in ethanol. Handsheets were fabricated in uncoated and CTS/NT-coated configurations, with coatings applied via spray coating. Chemical analysis revealed high holocellulose (93.39%) and alpha-cellulose (76.26%) contents, indicating effective delignification (3.65% residual lignin). FTIR spectroscopy confirmed the presence of cellulose and lignin in both the pulp and LCNF, as well as successful coating retention in handsheets. The handsheet incorporating 15 wt% LCNF loading with CTS/NT coating exhibited enhanced tensile index and folding endurance, though with reduced tear resistance. For optical properties, brightness improved while opacity remained stable. FE-SEM imaging revealed reduced porosity and confirmed the presence of a coating layer on treated samples. Notably, the CTS/NT coating significantly enhanced the barrier properties, achieving water contact angles of 116°–127°, compared to 0° in uncoated handsheets. These findings demonstrate the considerable potential of *B. vulgaris* pulp for sustainable paper products. The combined functionalization with LCNF and CTS/NT offers a biodegradable, high-performance alternative to synthetic materials, making it particularly suitable for eco-friendly applications in food, nutritional, and pharmaceutical packaging.

Introduction

Paper is a versatile and essential commodity in everyday life, valued for its affordability, biocompatibility, and biodegradability. However, the papermaking industry faces growing sustainability challenges, including deforestation, high water and energy consumption, and pollution from chemical processing (Jiang et al. 2021). While demand for printing and writing grades has declined, packaging paper and paperboard usage continue to dominate global consumption due to e-commerce and shifting consumer preferences toward eco-friendly materials. The global demand for paper packaging is projected to grow by 27% between 2021 and 2032, reaching 226 million tons (Statista 2023). The e-commerce packaging market was valued at USD 70.27 billion in 2022 and is expected to grow at a compound annual growth rate (CAGR) of 17.12%, reaching USD 340 billion by 2032 (Precedence Research Ltd. 2023).

Bamboo, particularly the species *Bambusa vulgaris* Schrad. ex J.C. Wendl, represents a promising fiber source due to its rapid growth, renewability, and high fiber quality, offering a sustainable alternative amid the decline of commercial softwood and hardwood species supplies. Unlike traditional wood sources, bamboo matures within 3–5 years and can be harvested without killing the plant, enabling continuous regeneration). The chemical composition of mature (> 3 years old) *B. vulgaris* is comparable to that of hardwoods, with 60–70% holocellulose, 20–25% pentosans, 20–30% hemicellulose and lignin, and other

minor elements such as resin, tannins, waxes, and inorganic salts (Junior et al. 2019; Khantayawunong et al. 2022). It has a fiber length of 1.74 to 2.16 mm, a width of 22 to 24 μm, and cell wall thickness of 15 to 17 μm Khantayanuwong et al. 2022), which indicate that fibers are long, thick-walled, narrow, and have a small lumen, which contribute to its rigidity and strength. Due to its high cellulose content and favorable fiber dimensions, *B. vulgaris* can serve as an excellent raw material for paper and textile production.

Over the years, the pulp and papermaking industry has continued to evolve to address sustainability issues while achieving desirable properties for specific end-use applications. Nanotechnology, in particular, has garnered significant attention over the last two decades due to its impact on enhancing materials across numerous industries (Balea et al. 2020). Nanocellulose-based additives, in the forms of cellulose nanofibers (CNF) and cellulose nanocrystals (CNC), have been widely adopted to improve paper properties (Samyn et al. 2018; Tang et al. 2020). CNF has attracted attention in papermaking due to its longer chain length and diameter of 10–100 nm, which provides flexibility and larger surface areas compared to CNCs (Thomas et al. 2018; Yan et al. 2022). However, CNF production often involves extensive chemical treatments to remove lignin and hemicellulose, resulting in high processing costs and chemical waste generation (Yan et al. 2022). To address this challenge, researchers have focused on lignocellulosic nanofibers (LCNF), which retain both lignin and cellulose, offering a more environmentally friendly alternative (Delgado-Aguilar et al. 2016; Demuner et al. 2019; Espinosa et al. 2017).

Lignin, a naturally occurring biopolymer in plant cell walls, contributes to excellent mechanical properties, hydrophobicity, and thermal stability (Espinosa et al. 2017; Zhang et al. 2022). Delgado-Aguilar et al. (2016) reported that LCNF with lignin content of 2–3% improved the tensile index of paper products. Demuner et al. (2019) evaluated the incorporation of LCNF and CNF into kraft liners and sack kraft papers, finding that LCNFs exhibited higher thermal stability and improved tensile and burst indices compared to CNFs. These results suggest that LCNFs are promising additives for paper products and merit further investigation under different processing and application conditions.

Surface functionalization using biodegradable coatings is gaining interest as a strategy to enhance paper's barrier properties for packaging applications. Conventional coatings often involve synthetic polymers and fluorochemicals, which contribute to environmental pollution (Lavoine and Bergström 2017). As an alternative, chitosan (CTS), a biopolymer derived from exoskeletons of crustaceans, and nano-titanium dioxide (NT), known for its antimicrobial and UV-protective properties, offer a bio-based and environmentally friendly coating solution (Toro et al. 2022). This combination also improves mechanical strength properties of paper and imparts hydrophobicity and flame retardancy to cotton-based textiles (Tang et al. 2016; Becenen and Erdogan 2022).

This research work aimed to investigate the effects of functionalization with LCNF addition and CTS/NT surface coating on the selected properties of *B. vulgaris* handsheets. The physical properties examined included grammage, apparent thickness, apparent density, tensile index, tear index, folding endurance,

and optical properties (brightness and opacity). Morphological characterization was conducted using Field Emission Scanning Electron Microscopy (FE-SEM). The chemical characteristics were assessed by determining the holocellulose, alpha-cellulose, hemicellulose, and residual lignin contents through proximate chemical analysis (PCA) while Fourier-transform infrared spectroscopy (FTIR) was employed to confirm the presence of chemical constituents and coating materials. Additionally, the hydrophobic performance of the CTS/NT coating was evaluated by measuring water contact angle (WCA). By integrating LCNF reinforcement with CTS/NT surface modification, this study seeks to enhance various properties of bamboo-based paper, thereby promoting the potential of *B. vulgaris* as a sustainable raw material for value-added papermaking applications.

Experimental

Materials

Mature *B. vulgaris* poles, aged 3–5 years old, were harvested from the bambusetum of Department of Environment Natural Resources - Ecosystems Research and Development Bureau (DENR-ERDB) in Laguna, Philippines. Analytical grades of sodium hydroxide (Merck), titanium dioxide nanoparticles (Sigma Aldrich), sodium sulfide (JT Baker), and chitosan (Merck) were obtained from local suppliers.

Methods

The experimental procedure is summarized in Fig. 1, and each step is described in detail in the following subsections.

Pulping of bamboo chips

Kraft pulping was carried out at a 5:1 liquor-to-bamboo ratio with 25% sulfidity and 20% active alkali. After 10 min of pre-mixing, the digester was heated from room temperature to 170°C and maintained for 120 min to complete the cook.

Production of LCNF

Unbleached BKP suspension in distilled water (0.78% w/v) was processed using a supermass colloider (MKCA6-2J, Masuko Sangyo Co. Ltd.) equipped with ceramic nonporous discs. The clearance was set to 1 (passes 1–2), 3 (passes 3–4), 5 (passes 5–6), 7 (passes 7–8), 9 (passes 9–10), and 10 (passes 11–15). The obtained LCNF was freeze-dried (Freezone Benchtop, Labconco) at 0.000 mbar and − 50°C.

Chemical characterization of BKP and LCNF

The chemical composition of the unbleached pulps was analyzed via proximate chemical analysis (PCA). Holocellulose and α-cellulose were determined sequentially by delignifying pulps with sodium

chlorite at 75°C for 3.25 h, followed by NaOH treatment (15.6%) to isolate α-cellulose. Residual lignin was measured as acid-insoluble lignin using 72% sulfuric acid hydrolysis. To compare BKP and LCNF, samples were analyzed by FTIR spectroscopy (IRPrestige 21, Shimadzu) in transmission mode over 500–4000 cm^{-1}.

Coating formulation

The chitosan (CTS)/nano-titanium dioxide (NT) coating formulation was adapted from Tang et al. (2016). CTS powder (2 g, 99% purity) was dispersed in 3% (v/v) acetic acid (200 mL) and heated to 60°C with magnetic stirring at 1000 rpm. After 30 min, glycerol (2 mL) was added as a plasticizer, and stirring continued until homogeneous. NT particles (10 wt% of CTS) were dispersed in ethanol (10 mL) for 30 min at 350 rpm, then added to the CTS suspension and stirred for 60 min at 1000 rpm. The mixture was cooled to room temperature for viscosity measurement (≈ 100 cP) and applied to handsheets using a commercial airbrush with a 0.05 mm nozzle.

Handsheet formation

Handsheets were prepared following ISO 5269-1. BKP and freeze-dried LCNF were diluted in distilled water to 1.2% consistency. For samples without LCNF, pulps were disintegrated for 10,000 revolutions and formed using a 120-mesh (~ 125 μm) wire. When LCNF was incorporated, the slurry was disintegrated for 45,000 revolutions to ensure uniform dispersion, with a 180-mesh (~ 80 μm) nylon filter placed over the forming wire for nanofiber retention. During couching, the roll was moved back and forth five times under its own weight. Wet handsheets (≤ 10 per batch) were pressed at 50 psi for 5 min, then air-dried in rings for 24 h and conditioned at 23 ± 1°C and 50 ± 2% RH (ISO 187) prior to testing.

Surface coating application

The CTS/NT coating suspension was applied via surface treatment, following the spray coating method adapted from Ogihara et al. (2012). A total of 10 mL of the coating suspension was sprayed onto the handsheets using an airbrush, with the pressure set at 50 psi and a spraying distance of 3 to 5 inches for uniform coverage. The coating was applied to the unglazed side of the handsheet to improve adhesion and underwent 24-hours of air-drying. Subsequently, the specimens were repressed under the same pressing conditions used during sheet-making and then transferred to the conditioning room, along with the uncoated samples, for property testing.

Handsheet characterization

Thirty handsheets were produced, with five replicates per treatment combination. Samples were classified by LCNF loading (0, 10, 15%)—denoted as LCNF-0, LCNF-10, and LCNF-15—and by surface coating, labeled as CO (coated) or UN (uncoated). Accordingly, treatments included UN-LCNF-0 (control), UN-LCNF-10, UN-LCNF-15, CO-LCNF-0, CO-LCNF-10, and CO-LCNF-15.

Following ISO 5270, five replicates per treatment were tested for structural, mechanical, and optical properties. Structural properties (grammage, coating retention, thickness, and density) were measured using an analytical balance (Kern 770) and a digimatic indicator (Mitutoyo ID series). Mechanical properties—tensile index, tear index, and folding endurance—were determined using an INSTRON 4444, a Frank-PTI Elmendorf tear tester (S53984), and an MIT folding endurance tester (QT-60140A). Optical properties (opacity and brightness) were measured with a Noviprofibre spectrophotometer (N5950B) per ISO 2471 and ISO 2470.

Morphological analysis of BKP, LCNF, and selected handsheets (UN-LCNF-0, UN-LCNF-10, UN-LCNF-15, CO-LCNF-0, CO-LCNF-15) was conducted via FE-SEM (JEOL JSM IT500HR) after platinum sputter coating (40 mA, 75 s). Chemical characteristics of representative coated and uncoated samples were further examined by FTIR spectroscopy to confirm CTS/NT coating retention.

Water contact angle measurement

The wettability of the coated handsheets was assessed using contact angle goniometry. Two 2 µL water droplets were placed 3 cm from the rupture point, and contact angles were recorded at 15, 30, 60, and 120 s. Droplet images were captured with a Dino-Lite digital microscope and analyzed using the Drop Snake plugin in ImageJ.

Data analysis

A two-factor factorial design—comprising LCNF loading and surface coating in a completely randomized setup was employed to evaluate the physical properties of the handsheets. The same analytical approach was applied to the WCA measurements of the coated samples, with LCNF loading and holding time as factors. Resulting data were analyzed using analysis of variance (ANOVA) and Tukey's Honest Significant Difference (HSD) test at 95% confidence level.

Results and discussion

Analysis of the chemical composition

Fiber morphology

The FE-SEM micrographs revealed distinct morphological characteristics of the BKP and LCNF (Fig. 2a and 2b). Using ImageJ software, pulp macrofibers were measured to have an average diameter of 10µm. Notable defibrillation was observed in the LCNF, characterized by irregular fiber bundles and extensive branching of cellulose fibrils. The supermass colloider mechanism transformed the macrofibers through multiple processes: cutting them into shorter lengths, external delamination through shearing forces, and internal fibrillation via crushing and compression (Xie et al. 2018). This mechanical treatment

produced a highly refined fibrillar structure with significantly increased surface area, yielding nanofibers ranging from 42–98 nm in diameter.

Proximate chemical analysis

The PCA results of the bone-dry BKP are shown in Table 1. The holocellulose content (93.39%) was closely aligned with that of Moso bamboo kraft pulp (90.20%) reported by Chen et al. (2022) and comparable to the levels found in hardwood (91–95%) and softwood (91%) pulps documented by Buzala et al. (2017). These high holocellulose levels highlight the efficiency of the kraft process in retaining the essential cellulose and hemicellulose components of bamboo, which are critical for pulp strength and quality.

The residual lignin content (3.65%) was relatively low for unbleached pulps, falling in the lower end of the typical range of ~ 2 to 5% (Li et al. 2018). This indicates effective delignification during the kraft process and that pulps can be readily bleached to achieve higher brightness levels with minimal chemical consumption. Additionally, the lignin content was consistent with the recommendation by Delgado-Aguilar et al. (2016), who specified that lignin contents of ~ 2–3% are preferable for LCNF to improve paper strength properties.

Table 1
Proximate chemical analysis of the *B. vulgaris* kraft pulp.

Parameters (%)	
Holocellulose	93.39 (± 3.38)
Alpha-cellulose	76.26 (± 4.33)
Residual Lignin	3.65 (± 0.29)
Hemicellulose	19.75 (± 2.79)

FTIR analysis

The functional groups of cellulose and lignin in BKP and LCNF were confirmed through FTIR spectroscopy (Fig. 3), which highlighted the functional group region from 3800 cm^{-1} to 2700 cm^{-1} and fingerprint region spanning 1800 cm^{-1} to 700 cm^{-1}. The spectra for both kraft pulp and LCNF were notably similar, with prominent peaks at 3331 cm^{-1} and 2895 cm^{-1} associated with OH and CH stretching, respectively, confirming the predominance of cellulose, hemicellulose, and lignin (Biswas et al. 2022). Peaks at 1161 cm^{-1} and 896 cm^{-1} were attributed to C-O-C glycosidic linkages (Tanpichai et al. 2022)d rock deformation (Jara et al. 2019) in cellulose. The lower transmittance values observed in the LCNF spectrum indicated stronger absorption by functional groups, suggesting a higher abundance of hydroxyl groups and increased cellulose content while confirming the preservation of the cellulose structure (Jara et al., 2019), suggesting a higher abundance of hydroxyl groups and increased cellulose content while confirming the preservation of the cellulose structure (Jara et al., 2019).

Lignin in bamboo species has been found to be similar to that of hardwoods, constant of both syringyl and guaiacyl units (Xiao et al. 2023). In both BKP and LCNF, residual lignin was detected on bands 1637 cm^{-1}, 1429 cm^{-1}, and 1315 cm^{-1} denoted as C = O stretching (Demuner et al. 2020), R-CH_2 group in the aromatic skeleton (Yu et al. 2022), and syringyl rings (Shi et al. 2019; Biswas et al. 2022), respectively. This was expected since LCNF was mechanically extracted from BKP and no chemical removal of residual lignin.

Figure 4 presents the FTIR spectra of the uncoated and coated handsheets with the CTS/NT coating components clearly detected. Since chitosan shares a similar structure with cellulose, its –OH groups, C–H stretching, and ether linkages were identified at bands 3300 cm^{-1}, 2895–2891 cm^{-1}, and 1161 cm^{-1}, respectively (Fig. 4a). The N–H stretching in chitosan was also detected at 3300 cm^{-1} (Ghasemi et al. 2017). The decreased intensity in these regions for coated samples may be attributed to the detection of chitosan functional groups on the sheet surface. Inorganic compounds such as TiO_2 are typically detected at lower wavelengths. In the FTIR spectra of the coated handsheets, TiO_2 was identified by absorbance peaks in the 580–420 cm^{-1} range as seen in Fig. 4b. This finding was consistent with previous studies (Jao et al. 2024; Toro et al. 2020) incorporating TiO_2 nanoparticles as surface coatings. CO-LCNF-15 exhibited deeper peak intensity compared to CO-LCNF-0, suggesting enhanced retention of TiO_2 nanoparticles on the fiber surface and indicating a thicker coating layer. The peaks associated with UN-LCNF-0 in the 580–420 cm^{-1} region can be attributed to bamboo's carbohydrate skeletal vibrations (Wiercigroch et al. 2017; Hong et al. 2021). Comparative analysis of transmittance at 430 cm^{-1} revealed the highest value for UN-LCNF-0 (64.14%), followed by CO-LCNF-0 (56.82%) and CO-LCNF-15 (44.44%), indicating successful surface modification of the handsheets through coating application, which altered their absorption behavior. The deeper vibrations in CO-LCNF-15 extended up to 500 cm^{-1}.

Physical properties

Structural properties: grammage, thickness, and density

The grammage, apparent thickness, and apparent density were measured to assess the structural characteristics of the handsheets (Fig. 5). The target grammage was set at 100 g/m², with actual values ranging from 99 g/m² to 112 g/m² (Fig. 5a). ANOVA revealed that both LCNF loading ($p = 0.00241$) and coating ($p = 0.0435$) had significant effects on grammage, whereas their interaction did not ($p = 0.4086$). The grammage measurements indicated effective retention of LCNF within the fiber network, which can be attributed to the beating process prior to sheet formation that promoted uniform dispersion of LCNF and enhanced bonding with the pulp macrofibers. TThe highest grammage was observed in CO-LCNF-15 handsheets (112.51 g/m²), which was statistically different from both coated and uncoated LCNF-10 samples but not from the control. This increase may be attributed to the higher LCNF content and larger surface area of nanofibers in CO-LCNF-15, which provided additional bonding sites for the CTS/NT_2 coating. As shown in Fig. 5b, coating retention improved with LCNF reinforcement.

The highest thickness among all handsheets was observed in the control (273.20 µm) (Fig. 5c). Addition of LCNF ($p < 0.0001$) significantly reduced thickness by 30.03% in UN-LCNF-10 (203.65 µm) and by

11.21% in UN-LCNF-15 (258.44 μm). This result indicates that LCNF enhanced fiber interactions and filled void spaces, leading to a more consolidated network and thinner sheets (Li et al. 2023). The less pronounced thickness reduction in UN-LCNF-15 was likely due to higher nanofiber content, which facilitated stronger interfiber bonds and resisted further fiber collapse. The CTS/NTcoating ($p = 0.0027$) had a significant effect only on LCNF-0 handsheets, where thickness decreased to 234.52 μm in CO-LCNF-0 (− 19.43%). This shrinkage is likely attributed to fiber hornification caused by rewetting and a second drying cycle during coating, where hornified fibers cannot fully recover their original dimensions (Hill et al. 2009). However, this effect was negligible in LCNF-reinforced handsheets, likely due to the minimal coating applied to a single side and the prior densification of the fiber network by LCNF, which may have already drawn fibers into closer contact before coating.

Significant differences in the apparent density were observed across both uncoated and coated handsheets, influenced by LCNF loading ($p < 0.0001$), coating ($p < 0.0001$) and their interaction ($p = 0.0151$). In Fig. 5d, UN-LCNF-10 achieved the highest apparent density (0.477 g/cm³), followed by UN-LCNF-15 (0.413 g/cm³), and the control (0.372 g/cm³). A similar trend was observed in the coated samples. This increase suggested that 10 wt% and 15 wt% of LCNF addition to the pulps resulted in a more compacted network due to defibrillated fibers filling gaps or void spaces (Balea et al. 2016; Pego et al. 2020). Furthermore, the CTS/NT coating appeared to embed more effectively within these compacted structures.

Mechanical properties: TSI, tear index, and FE

Tensile index (TSI), which represents tensile strength relative to grammage, is influenced by fiber strength, length, and interfiber bonding (Fellers 2009). ANOVA results showed that TSI was significantly affected by LCNF loading ($p < 0.0001$), coating application ($p < 0.0001$), and their interaction ($p = 0.00289$). Among uncoated samples, a significant increase was observed at 15 wt% LCNF loading, where UN-LCNF-15 achieved 17.23 ± 0.48 Nm/g, representing an improvement of 60.09% compared to UN-LCNF-0 (17.23 ± 0.48 Nm/g) (Fig. 6a). This aligned with previous findings (Kumar et al. 2014; Demuner et al. 2019; Bang et al. 2021), which reported that increasing nano/microfiber content in handsheet promoted higher tensile strength due to availability of larger surface area for intra- and intermolecular hydrogen bonding between fibers.

Application of the CTS/NT coating further enhanced TSI values across all samples, consistent with the findings by Tang et al. (2016). In the coating formulation, CTS was protonated in 3% (v/v) acetic acid, forming a polycationic structure. This provided additional hydrogen bonding through electrostatic interactions between protonated NH_3 + in CTS and the anionic OH- groups of cellulose, effectively bridging gaps between fibers (Bhardwaj et al. 2020; Zakaria et al. 2015; Tanpichai et al. 2022). TiO_2 nanoparticles, owing to their nanoscale size, were likely uniformly dispersed across the fiber matrix, promoting closer contact between CTS and cellulosic fibers (Ling et al. 2013; Tang et al. 2016), thereby reinforcing the fiber network.

The tear index measures a paper's resistance to tearing relative to its weight and is influenced by fiber length, bonding, and the number of fibers involved during rupture (Tozluoglu & Poyraz, 2016; Ehman et al., 2020). As shown in Fig. 6b, the tear index decreased with both LCNF addition and surface coating, contrasting the trend observed in tensile strength. The highest value was recorded for the unmodified handsheet (UN-LCNF-0) at 12.58 ± 0.61 mN·m²/g. Among uncoated samples, introducing 10 wt% LCNF reduced the tear index by 60.25% compared to the control.

This decline aligns with earlier findings (Vallejos et al., 2016; Ehman et al., 2020), where nanofiber incorporation mimicked the effects of intensive refining by forming a denser network at the expense of fiber length. The pronounced reduction in UN-LCNF-10 is likely due to thinner sheets and the presence of shorter, finer fibers, which limited tear energy dissipation. In UN-LCNF-15, stronger interfiber bonding may have mitigated the reduction in tear resistance.

Surface coating also lowered the tear index—by 37.19% and 32.97% in CO-LCNF-0 and CO-LCNF-15, respectively—compared to their uncoated versions. This contrasts with studies by Tang et al. (2016) and Zakaria et al. (2015), which reported improved tear properties after CTS/NT application. The discrepancy suggests that the specific coating formulation in this study may have increased fiber stiffness and brittleness, reducing paper flexibility and making it more prone to tearing. A similar outcome was reported by Krysztof et al. (2021), where coatings reduced tear resistance while improving tensile strength.

Folding endurance (FE), measured as the logarithm of double folds, was significantly affected by LCNF content ($p = 0.0001$), CTS/NT coating ($p < 0.0001$), and their interaction ($p = 0.00369$). As shown in Fig. 6c, the UN-LCNF-15 sample exhibited the highest FE (1.73; 89 double folds) among the uncoated group, demonstrating marked improvement over the control.

FE generally increases with refining, which enhances fiber flexibility and improves bonding area. However, this also shortens the fibers, which can reduce overall strength (Hubbe et al., 2007). In this case, the handsheets retained large fibers from *B. vulgaris*, while the 15 wt% LCNF acted like fines that filled gaps, tightened the fiber network, and facilitated more effective stress distribution. Similar results with higher nanofiber content have been reported (Yang et al. 2022).

Although thick coatings can reduce FE by limiting flexibility (Možina et al. 2013), the CTS/NT coating used here strengthened the paper. It enhanced FE by 172%, 192%, and 73% for CO-LCNF-0, CO-LCNF-10, and CO-LCNF-15 samples, respectively, compared to their uncoated versions. This improvement is likely attributed to the lightweight coating forming a protective layer that helped preserve fiber structure during folding cycles.

Optical properties

Opacity measurements were not significantly affected by LCNF ($p = 0.2169$) or its interaction with surface coating ($p = 0.8957$). The average opacity values ranged narrowly from 99.32% to 99.79% across all treatments (Fig. 7a), with no statistically significant differences observed. These results aligned with

previous findings (González et al. 2012; Pego et al. 2020; Kasmani and Samariha 2022), where nanofiber addition had minimal impact on opacity. Although defibrillation typically enhances light-scattering, it also increases the number of fiber contact points, which reduces the material's scattering efficiency, thus resulting in an overall reduction in opacity. However, as observed by Ahmadi et al. (2018), LCNFs derived from unbleached pulp tend to maintain high opacity due to their denser structure and lower transparency compared to CNFs from bleached sources.

Brightness was measured under the same conditions as opacity, with lower values anticipated due to the nature of unbleached pulps. Lignin, which contains chromophoric groups such as quinoids, aromatic ketones, stilbenes, and catechols (Azadfallah et al. 2008; Zhang et al. 2020), absorbs light in the violet and blue regions, resulting in the characteristic yellow appearance of unbleached pulps. Figure 7b shows that both uncoated and coated LCNF-15 handsheets exhibited highest brightness values at 35.80 ± 0.06% and 36.20 ± 0.14%., respectively. Relative to the control (34.01%), the brightness of UN-LCNF-15 increased by 1.79 percentage points (35.80%), while UN-LCNF-10 showed a smaller increase of 1.22 percentage points (35.23%).

The slight improvement was likely attributed to the enhanced light scattering from the high surface area of the LCNF (Hu et al. 2013; Pego et al. 2020) and its nanometric dimensions (< 100 nm), which are smaller than the wavelength of blue light (450–495 nm). This dimensional relationship suggests the occurrence of Rayleigh scattering, where incident light is neither absorbed nor transmitted, but instead diffusely reflected outward (Huang et al. 2023). Although TiO_2 nanoparticles were expected to further enhance brightness and opacity, no significant effects from coating ($p = 0.1654$ and $p = 0.1256$, respectively) were observed for either property. This may be attributed to the limited amount of TiO_2 applied, which was intentionally kept low to preserve mechanical strength, as excessive TiO_2 loading (> 10 wt% of chitosan) may negatively affect sheet strength (Tang et al., 2016).

Morphological properties

SEM micrographs revealed distinct structural differences among the handsheet treatments. UN-LCNF-0 handsheets (Fig. 8a) exhibited a more porous and open fiber network, while the LCNF addition in UN-LCNF-10 and UN-LCNF-15 (Figs. 8b and 8c) resulted in a more compact morphology. Notably, UN-LCNF-15 displayed a well-developed LCNF webbing, with nanofibers visibly adhering to macrofibers and bridging gaps in the matrix, demonstrating a more interconnected fiber network. Upon coating application, fibers in CO-LCNF-0 and CO-LCNF-15 (Figs. 8d and 8e) appeared more flattened, indicating that CTS/NT coating facilitated further fiber consolidation. A surface coating film was observed in both coated samples, though it was more prominent in CO-LCNF-15, likely due to the increased surface area and bonding sites provided by the nanofiber-reinforced structure, consistent with the findings of Tang et al. (2016).

Wettability

The application of the CTS/NT coating significantly enhanced the hydrophobicity of the handsheets. While uncoated samples were highly hydrophilic with water immediately absorbed by the cellulosic fibers, the coated handsheets demonstrated hydrophobicity with WCA exceeding 90° (Fig. 9). This outcome is consistent with findings of Tanpichai et al. (2022) using a single-layer coating. Statistical analysis confirmed that both LCNF loading and holding time significantly influenced WCA values ($p < 0.0001$). CO-LCNF-15 and CO-LCNF-10 showed significantly higher WCAs compared to CO-LCNF-0 after 15s holding time (Fig. 10). Notably, WCA of CO-LCNF-0 and CO-LCNF-10 decreased more rapidly with increased holding time, while CO-LCNF-15 maintained significantly higher contact angles even at 60s, suggesting superior water resistance.

The improved hydrophobicity in LCNF-reinforced handsheets is attributed to enhanced coating retention and the inherent properties of the coating components. TiO_2 nanoparticles, being water-insoluble, impede water penetration by promoting hydrogen bonding with their surface rather than with the cellulosic fibers (Jao et al., 2024). Furthermore, the low-molecular-weight chitosan likely reoriented its polar groups toward the sheet surface or fiber walls, reducing their exposure to water and retarding WCA degradation over time (Tanpichai et al. 2022). The synergistic effects of CTS and NT in the coating formulation resulted in higher contact angles (116° to 127°) for the coated handsheets compared to previous studies that employed individual coatings of CTS (66° to 108°; Tanpichai et al. 2022) and NT (64° to 93°; Jao et al. 2024).

Conclusion

This study demonstrated the viability of unbleached *Bambusa vulgaris* as a sustainable fiber source for pulp and papermaking due to its high cellulose content and low residual lignin following kraft pulping. The incorporation of lignocellulose nanofibers (LCNF) enhanced fiber bonding and densified the sheet structure, with 15 wt% loading (LCNF-15) yielding the most notable improvements in tensile strength and folding endurance. Subsequent surface coating with CTS/NT further augmented the mechanical performance, with CO-LCNF-15 achieving the highest tensile index (44.65 ± 1.58 Nm/g) and folding endurance (logfold = 3.01), along with a marked increase in hydrophobicity (water contact angle = 126.35°).

However, these enhancements in strength were accompanied by reduced tear resistance, particularly at 10 wt% LCNF loading and upon application of the coating layer, likely due to fiber shortening effects. Optical characteristics such as brightness showed slight improvement with LCNF addition, while opacity remained largely unchanged across all treatments. FTIR and FE-SEM analyses confirmed the successful integration and morphological modifications of LCNF and CTS/NT coatings on the handsheet surfaces.

Overall, the synergistic approach of LCNF reinforcement combined with CTS/NT surface coating presents a promising strategy to enhance the mechanical and barrier properties of bamboo-derived paper. This dual functionalization offers potential for developing sustainable, high-performance paper

products suitable for specialized packaging applications where enhanced strength and water resistance are critical requirements.

Declarations

Competing Interests:

There are no conflicts of interest to disclose that are relevant to the research and writing of the manuscript.

Ethics Approval:

The harvesting of *Bambusa vulgaris* poles was authorized by the Department of Environment and Natural Resources – Ecosystems Research and Development Bureau in Laguna, Philippines. The hauling and transportation permit for the harvested poles was granted by the University of the Philippines Los Baños – Makiling Center for Mountain Ecosystem (MCME). No human or animal subjects were involved in this research.

Funding:

This research was supported by the DOST-PCAARRD-funded projects of Asst. Prof. R.D. Manalo, titled "Valorization of Bamboo Processing Wastes for Adhesive and Coating Applications" and "Production, Characterization, and Potential Applications of Biodegradable Plastic from Bamboo."

Author Contribution

This manuscript is drafted based on the thesis work of M.G.M Macalinao as a partial fulfillment of the requirements for her MSc. in Forestry: Wood Science and Technology at UPLB. Conceptualization, data collection, analysis, and drafting of the initial manuscript were carried out by M.G.M. Macalinao. R.D. Manalo supervised the work, contributed to the methodological design, and provided critical revisions to the manuscript. J. O. Grande-Flores played a major role in reviewing and editing the manuscript, while J. D. Villanueva-Peyraube contributed to the review process.

Acknowledgement

The authors gratefully acknowledge the Pulp and Paper Laboratory of the Forest Products Research and Development Institute, especially Ms. A.B. Habon and Ms. S.K. Siapno-Pangan for the conduct of the physical tests, and Mr. R. Mariñas, Mr. S. Balmedina, and Mr. R.J. Pangan for their assistance during pulping and handsheet formation. Ms. M. G.M. Macalinao also acknowledges the Department of Science

and Technology–Science Education Institute (DOST-SEI) through the Accelerated Science and Technology Human Resource Development Program (ASTHRDP) for financial support during her graduate studies. Special appreciation is extended to Mr. J.M. Abogador for providing the original equipment artwork used in the methodology section.

References

1. Ahmadi M, Hedjazi S, Yousefi H (2018) Comparative properties of nanofibers produced using unbleached and bleached wheat straw pulps. Nord Pulp Pap Res J 33(3):439–447. https://doi.org/10.1515/npprj-2018-3024
2. Azadfallah M, Mirshokraei SA, Latibari AJ (2008) Photodegradation of acidolysis lignin from BCMP. Molecules 13(12):3129–3139. https://doi.org/10.3390/molecules13123129
3. Balea A, Merayo N, Fuente E, Delgado-Aguilar M, Mutjé P, Blanco A, Negro-Álvarez C (2016) Valorization of corn stalk by the production of cellulose nanofibers to improve recycled paper properties. BioResources 11(2):3416–3431. https://doi.org/10.15376/biores.11.2.3416-3431
4. Balea A, Fuente E, Monte MC, Merayo N, Campano C, Negro C, Blanco Á (2020) Industrial application of nanocelluloses in papermaking: A review of challenges, technical solutions, and market perspectives. Molecules 25(3):526. https://doi.org/10.3390/molecules25030526
5. Bang J, Lee H, Yang Y, Oh JK, Kwak HW (2021) Nano/micro hybrid bamboo fibrous preforms for robust biodegradable fiber reinforced plastics. Polymers 13(4):636. https://doi.org/10.3390/polym13040636
6. Becenen N, Erdoğan S (2022) Chitosan and nano-TiO_2 coating improves the flame retardancy of dyed and undyed denim fabrics by increasing the charring. J Ind Text 51(1_suppl):1252S–1278S. https://doi.org/10.1177/15280837221099632
7. Biswas S, Rahaman T, Gupta P, Mitra R, Dutta S, Kharlyngdoh E, et al (2022) Cellulose and lignin profiling in seven economically important bamboo species of India by anatomical, biochemical, FTIR spectroscopy and thermogravimetric analysis. Biomass Bioenergy 158:106362. https://doi.org/10.1016/j.biombioe.2022.106362
8. Buzała KP, Kalinowska H, Przybysz P, Małachowska E (2017) Conversion of various types of lignocellulosic biomass to fermentable sugars using kraft pulping and enzymatic hydrolysis. Wood Sci Technol 51(4):873–885. https://doi.org/10.1007/s00226-017-0916-7
9. Chen H, Wang Y, Qiu J, Song J, Wang J, Liu M, et al (2022) Properties and application of kraft pulp prepared from waste bamboo powder. BioResources 17(4):6262–6276. https://doi.org/10.15376/biores.17.4.6262-6276
10. Delgado-Aguilar M, González I, Tarrés Q, Pèlach MÀ, Alcalà M, Mutjé P (2016) The key role of lignin in the production of low-cost lignocellulosic nanofibres for papermaking applications. Ind Crops Prod 86:295–300. https://doi.org/10.1016/j.indcrop.2016.04.010
11. Demuner I, Colodette JL, Gomes FJB, Oliveira RC (2019) Production and characterization of CNF and LCNF, and manufacture of LCNF-nanostructured packaging papers. Chem Eng Trans 73:43–48.

https://doi.org/10.3303/cet1973008

12. Ehman NV, Felissia FE, Tarrés Q, Vallejos ME, Delgado-Aguilar M, Mutjé P, Area M (2020) Effect of nanofiber addition on the physical–mechanical properties of chemimechanical pulp handsheets for packaging. Cellulose 27(18):10811–10823. https://doi.org/10.1007/s10570-020-03207-5
13. Espinosa E, Domínguez-Robles J, Sánchez R, Tarrés Q, Rodríguez A (2017) The effect of pre-treatment on the production of lignocellulosic nanofibers and their application as a reinforcing agent in paper. Cellulose 24(6):2605–2618. https://doi.org/10.1007/s10570-017-1281-2
14. Fellers C (2009) Paper physics. In: Ek M, Gellerstedt G, Henriksson G (eds) Paper chemistry and paper physics. Walter de Gruyter, Berlin, pp 25–68. https://doi.org/10.1515/9783110213461.25
15. Ghasemi M, Amoozadeh A, Kowsari E (2017) Chitosan-functionalized nano-titanium dioxide: A novel and highly efficient nanocatalyst for the synthesis of 2,4,5-trisubstituted imidazoles under solvent-free conditions. React Kinet Mech Catal 120(2):605–617. https://doi.org/10.1007/s11144-016-1114-6
16. González I, Boufi S, Pèlach MA, Alcalà M, Vilaseca F, Mutjé P (2012) Nanofibrillated cellulose as paper additive in eucalyptus pulps. BioResources 7(4):5167–5180. https://doi.org/10.15376/biores.7.4.5167-5180
17. Hill C, Norton A, Newman G (2009) The water vapor sorption behavior of natural fibers. J Appl Polym Sci 112(3):1524–1537. https://doi.org/10.1002/app.29725
18. Hong T, Yin JY, Nie SP, Xie MY (2021) Applications of infrared spectroscopy in polysaccharide structural analysis: Progress, challenge and perspective. Food Chem X 12:100168. https://doi.org/10.1016/j.fochx.2021.100168
19. Hu L, Zheng G, Yao J, Liu N, Weil B, Eskilsson M, et al (2013) Transparent and conductive paper from nanocellulose fibers. Energy Environ Sci 6(2):513–518. https://doi.org/10.1039/c2ee23635d
20. Huang Y, Kasuga T, Nogi M, Koga H (2023) Clearly transparent and air-permeable nanopaper with porous structures consisting of TEMPO-oxidized cellulose nanofibers. RSC Adv 13(31):21494–501. https://doi.org/10.1039/D3RA03840H
21. Hubbe MA, Venditti RA, Rojas OJ (2007) What happens to cellulosic fibers during papermaking and recycling? A review. BioResources 2(4): 739–788.
22. ISO (2022) ISO 187:2022. Paper, board and pulps—Standard atmosphere for conditioning and testing and procedure for monitoring the atmosphere and conditioning of samples. International Organization for Standardization, Geneva. https://www.iso.org/standard/80311.html
23. ISO (1976) ISO 3787:1976. Wood—Test methods—Determination of ultimate stress in compression parallel to grain. International Organization for Standardization, Geneva. https://www.iso.org/standard/9313.html
24. ISO (2001) ISO 5267-2:2001. Pulps—Determination of drainability—Part 2: "Canadian Standard" freeness method. International Organization for Standardization, Geneva. https://www.iso.org/standard/26707.html

25. ISO (2005) ISO 5269-1:2005. Pulps—Preparation of laboratory sheets for physical testing—Part 1: Conventional sheet-former method. International Organization for Standardization, Geneva. https://www.iso.org/standard/39340.html
26. ISO (2022) ISO 5270:2022. Pulps—Laboratory sheets—Determination of physical properties. International Organization for Standardization, Geneva. https://www.iso.org/standard/76079.html
27. ISO (2016) ISO 2470-1:2016. Paper, board and pulps—Measurement of diffuse blue reflectance factor—Part 1: Indoor daylight conditions (D65 illumination). International Organization for Standardization, Geneva. https://www.iso.org/standard/69090.html
28. ISO (2008) ISO 2471:2008. Paper and board—Determination of opacity (paper backing)—Diffuse reflectance method. International Organization for Standardization, Geneva. https://www.iso.org/standard/39771.html
29. Jao CMR, Grande-Flores JO, Manalo RD. (2024). Surface modification of TiO2 with MPS and its effects on the wettability and physical properties of Kawayan Kiling (Bambusa vulgaris Schrad ex. Wendl) handsheets. TAPPI Journal 23(4): 209–220. https://doi.org/10.32964/tj23.4.209
30. Jara AA, Razal RA, Migo VP, Acda MN, Calderon MM, Florece LM, Peralta EK (2019) Production of nanocellulose and biocomposites from Kawayan Kiling (Bambusa vulgaris Schrader ex Wendland) shoots. Ecosyst Dev J 10(1–2):1–10
31. Jiang S, Li B, Shen Y (2021). The influence of pulp and paper industry on environment. E3S Web Conf 308:02007. https://doi.org/10.1051/e3sconf/202130802007
32. Júnior EAB, Lengowski EC, de Andrade AS, Venson I, Klock U, da Silva-Júnior FG, Gonçalez JC, de Muñiz GIB (2019). Bamboo kraft pulping. Adv For Sci 6(4):791. https://doi.org/10.34062/afs.v6i4.8361
33. Kasmani JE, Samariha A (2022) Effects of different levels of nanocellulose and chemical pulp on the optical and mechanical properties of money paper made with bottom combers pulp. BioResources 17(2):2667–2679. https://doi.org/10.15376/biores.17.2.2667-2679
34. Khantayanuwong S, Yimlamai P, Chitbanyong K, Wanitpinyo K, Pisutpiched S, Sungkaew S, Sukyai P, Puangsin B (2022) Fiber morphology, chemical composition, and properties of kraft pulping handsheet made from four Thailand bamboo species.. Journal of Natural Fibers, 20(1).
35. Kumar A, Singh SP, Singh AK (2014) Preparation and characterization of cellulose nanofibers from bleached pulp using a mechanical treatment method. TAPPI J 13(5):25–31
36. Krysztof M, Olejnik K, Kulpiński P, Erdman A, Sąsiadek E (2021) A comparative study of the effect of cellulose-based deep coating and pulp refining on the structural and mechanical properties of paper. BioResources 16(3):5376–5389. https://doi.org/10.15376/biores.16.3.5376-5389
37. Lavoine N, Bergström L (2017) Nanocellulose-based foams and aerogels: processing, properties, and applications. J Mater Chem A 5(31):16105–16117. https://doi.org/10.1039/c7ta02807e
38. Li Y, Li B, Mo W, Yang W, Wu S (2018) Influence of residual lignin and thermal drying on the ultrastructure of chemical hardwood pulp and its enzymatic hydrolysis properties. Cellulose 26(3):2075–2085. https://doi.org/10.1007/s10570-018-2184-6

39. Li H, Kulachenko A, Mathew AP, Stoltz RB, Sevastyanova O (2023) Enhancing the Strength and Flexibility of Microfibrillated Cellulose Films from Lignin-Rich Kraft Pulp. ACS Sustain Chem Eng 11(47):16793–805. https://doi.org/10.1021/acssuschemeng.3c05086
40. Ling Y, Luo Y, Luo J, Wang X, Sun R (2013) Novel antibacterial paper based on quaternized carboxymethyl chitosan/organic montmorillonite/Ag NP nanocomposites. Ind Crops Prod 51:470–479. https://doi.org/10.1016/j.indcrop.2013.09.040
41. Možina K, Pracek S, Bukošek V (2013) Linear behaviour of one-side coated paper: Anisotropy. Cellul Chem Technol 47(5–6): 461–468.
42. Ogihara H, Xie J, Okagaki J, Saji T (2012) Simple method for preparing superhydrophobic paper: Spray-deposited hydrophobic silica nanoparticle coatings exhibit high water-repellency and transparency. Langmuir 28(10):4605–4608. https://doi.org/10.1021/la204492q
43. Pego MFF, Bianchi ML, Yasumura PK (2020) Nanocellulose reinforcement in paper produced from fiber blending. Wood Sci Technol 54(6):1587–1603. https://doi.org/10.1007/s00226-020-01226-w
44. Precedence Research Ltd (2023) E-commerce packaging market size to attain USD 341.27 billion by 2032. https://www.precedenceresearch.com/ecommerce-packaging-market. Accessed 10 June 2024
45. Samyn P, Barhoum A (2018) Engineered nanomaterials for papermaking industry. Elsevier, Amsterdam, pp 245–277. https://doi.org/10.1016/b978-0-323-51255-8.00009-4
46. Shi Z, Xu G, Deng J, Dong M, Murugadoss V, Liu C, Shao Q, Wu S, Guo Z (2019) Structural characterization of lignin from D. sinicus by FTIR and NMR techniques. Green Chem Lett Rev 12(3):235–243. https://doi.org/10.1080/17518253.2019.1627428
47. Statista Research Department (2024) Topic: Global pulp industry. https://www.statista.com/topics/7345/pulp-industry/#topic
48. Tang Y, Hu X, Zhang X, Guo D, Zhang J, Kong F (2016) Chitosan/titanium dioxide nanocomposite coatings: Rheological behavior and surface application to cellulosic paper. Carbohydr Polym 151:752–759. https://doi.org/10.1016/j.carbpol.2016.06.023
49. Tang RH, Li M, Liu LN, Zhang SF, Alam N, You M, Ni YH, Li ZD (2020) Chitosan-modified nitrocellulose membrane for paper-based point-of-care testing. Cellulose 27(7):3835–3846. https://doi.org/10.1007/s10570-020-03031-x
50. Tanpichai S, Srimarut Y, Woraprayote W, Malila Y (2022) Chitosan coating for the preparation of multilayer coated paper for food-contact packaging: Wettability, mechanical properties, and overall migration. Int J Biol Macromol 213:534–545. https://doi.org/10.1016/j.ijbiomac.2022.05.193
51. Thomas B, MC B, AK B, H R, Raj RM, Joy J, Moores A, Drisko GL, Sánchez C (2018) Nanocellulose, a versatile green platform: From biosources to materials and their applications. Chem Rev 118(24):11575–11625. https://doi.org/10.1021/acs.chemrev.7b00627
52. Toro RG, Diab M, De Caro T, Al-Shemy M, Adel A, Caschera D (2020) Study of the effect of titanium dioxide hydrosol on the photocatalytic and mechanical properties of paper sheets. Materials 13(6):1326. https://doi.org/10.3390/ma13061326

53. Tozluoglu A, Poyraz B (2016) Effects of cellulose micro/nanofibers as paper additives in kraft and kraft–$NaBH_4$ pulps. Nord Pulp Pap Res J 31(4):561–572. https://doi.org/10.3183/npprj-2016-31-04-p561-572
54. Vallejos ME, Felissia FE, Area MC, Ehman NV, Tarrés Q, Mutjé P (2016) Nanofibrillated cellulose (CNF) from eucalyptus sawdust as a dry strength agent of unrefined eucalyptus handsheets. Carbohydr Polym 139:99–105. https://doi.org/10.1016/j.carbpol.2015.12.004
55. Wiercigroch E, Szafraniec E, Czamara K, Pacia MZ, Majzner K, Kochan K, Kaczor A, Baranska M, Malek K (2017) Raman and infrared spectroscopy of carbohydrates: A review. Spectrochim Acta A Mol Biomol Spectrosc 185:317–335. https://doi.org/10.1016/j.saa.2017.05.045
56. Xiao L, Lv Y, Yang Y, Zou S, Shi Z, Sun R (2023) Unraveling the lignin structural variation in different bamboo species. Int J Mol Sci 24(12):10304. https://doi.org/10.3390/ijms241210304
57. Xie H, Du H, Yang X, Si C (2018) Recent strategies in preparation of cellulose nanocrystals and cellulose nanofibrils derived from raw cellulose materials. Int J Polym Sci 2018:1–25. https://doi.org/10.1155/2018/7923068
58. Yan M, Wu T, Ma J, Lu H, Zhou X (2022) A systematic study of lignocellulose nanofibrils (LCNF) prepared from wheat straw by varied acid pretreatments. Ind Crops Prod 185:115126. https://doi.org/10.1016/j.indcrop.2022.115126
59. Yang B, Zhou Q, Zhang M, Wang L, Li W, Lu P (2022) Highly foldable, robust and water-resistant cellulose specialty paper reinforced by aramid nanofibers. Cellulose 29(3):2033–2045. https://doi.org/10.1007/s10570-021-04404-6
60. Yu H, Gui C, Ji Y, Li X, Rao F, Huan W, Li L (2022) Changes in chemical and thermal properties of bamboo after delignification treatment. Polymers 14(13):2573. https://doi.org/10.3390/polym14132573
61. Zakaria S, Chin HC, Ahmad WHW, Kaco H, Soon WC, Chi HC (2015) Mechanical and antibacterial properties of paper coated with chitosan. Sains Malays 44(6):905–911. https://doi.org/10.17576/jsm-2015-4406-18
62. Zhang Q, Ma L, Zhang X, Zhang L, Wang Z (2022) Lignocellulose nanofiber/polylactic acid (LCNF/PLA) composite with internal lignin for enhanced performance as 3D printable filament. Ind Crops Prod 178:114590. https://doi.org/10.1016/j.indcrop.2022.114590

Figures

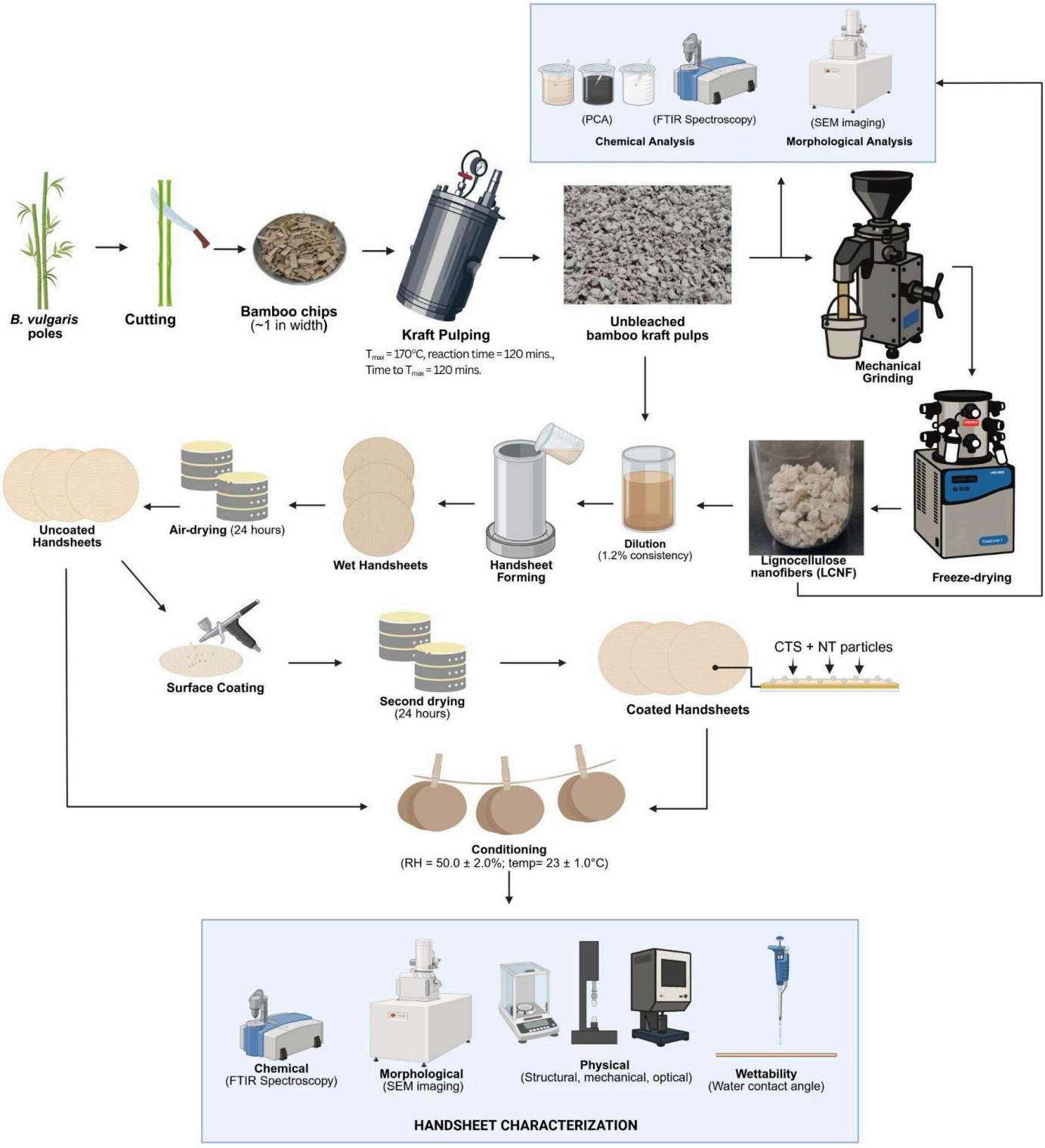


Figure 1

Schematic diagram of the LCNF reinforcement and CTS/NT coating of *B. vulgaris* handsheets

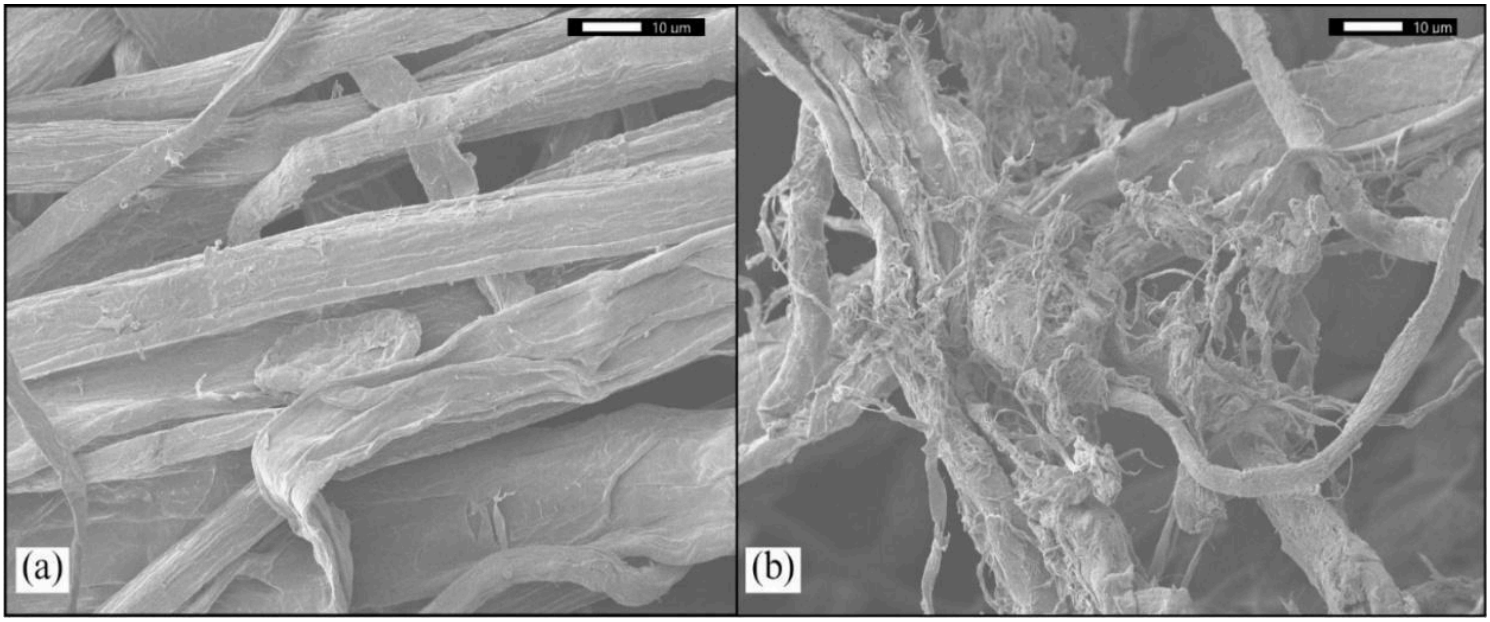


Figure 2

FE-SEM micrographs of (a) BKP and (b) LCNF under 1000x magnification.

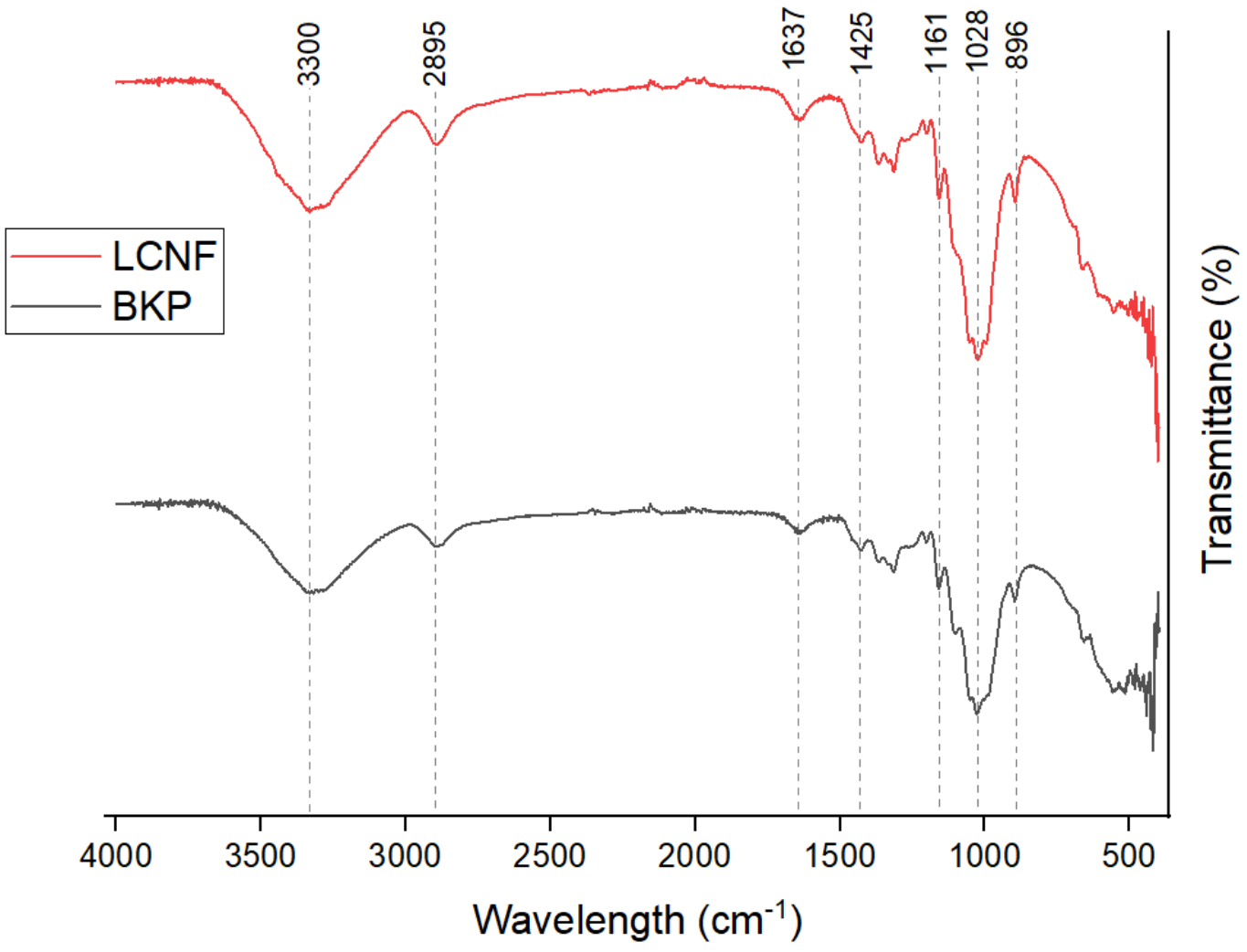


Figure 3

FTIR spectra of BKP and LCNF

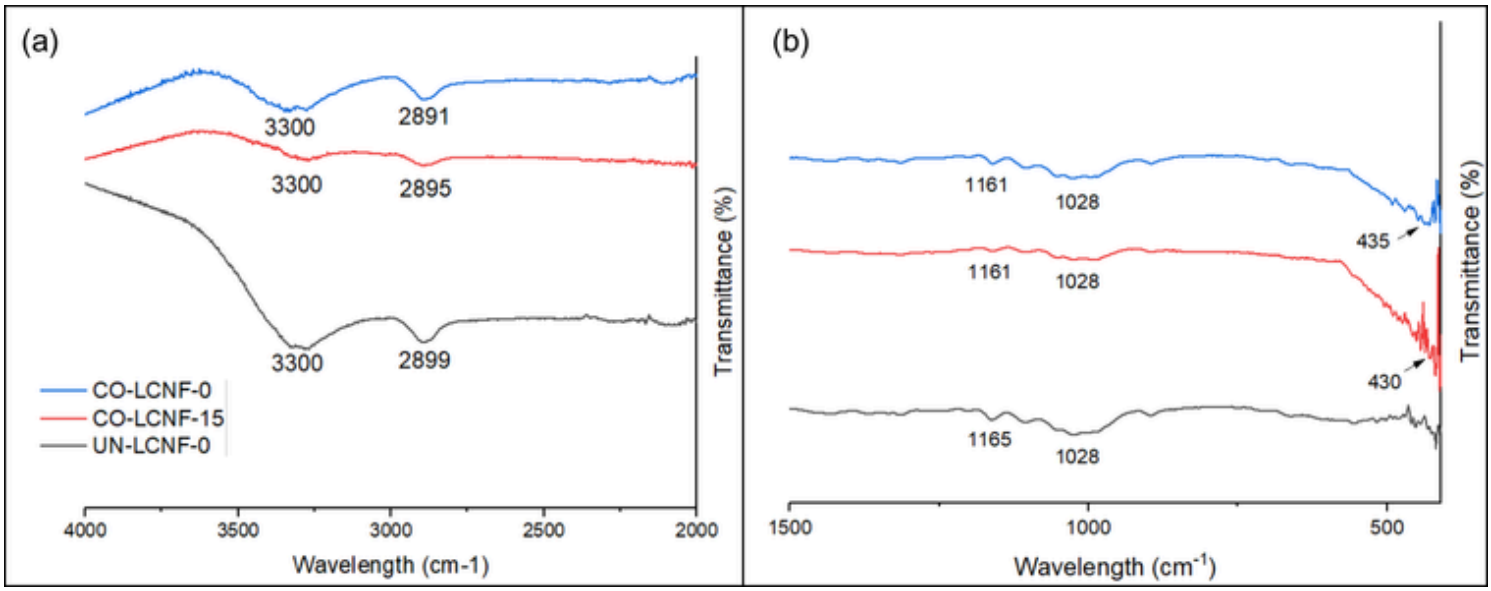


Figure 4

FTIR spectra of uncoated (UN-LCNF-0) and coated (CO-LCNF-0 and CO-LCNF-15) handsheets in: (a) functional group region and (b) fingerprint region

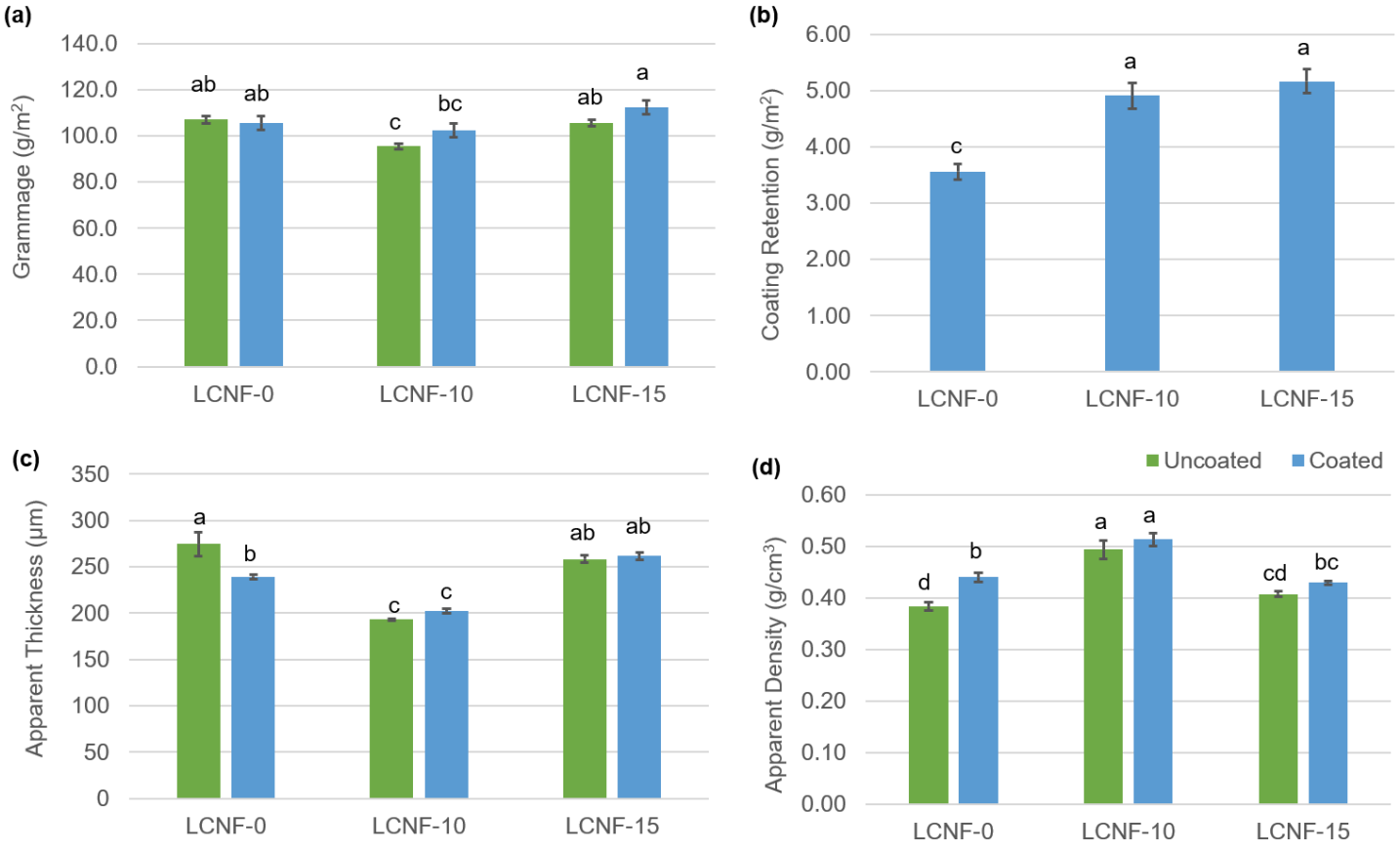


Figure 5

Structural properties of coated and uncoated handsheets with 0, 10, and 15% LCNF loading: a) grammage; b) coating retention, c) apparent thickness, and d) apparent density. Note: Columns with common letters are not significantly different (Tukey's HSD test, $p \leq 0.05$).

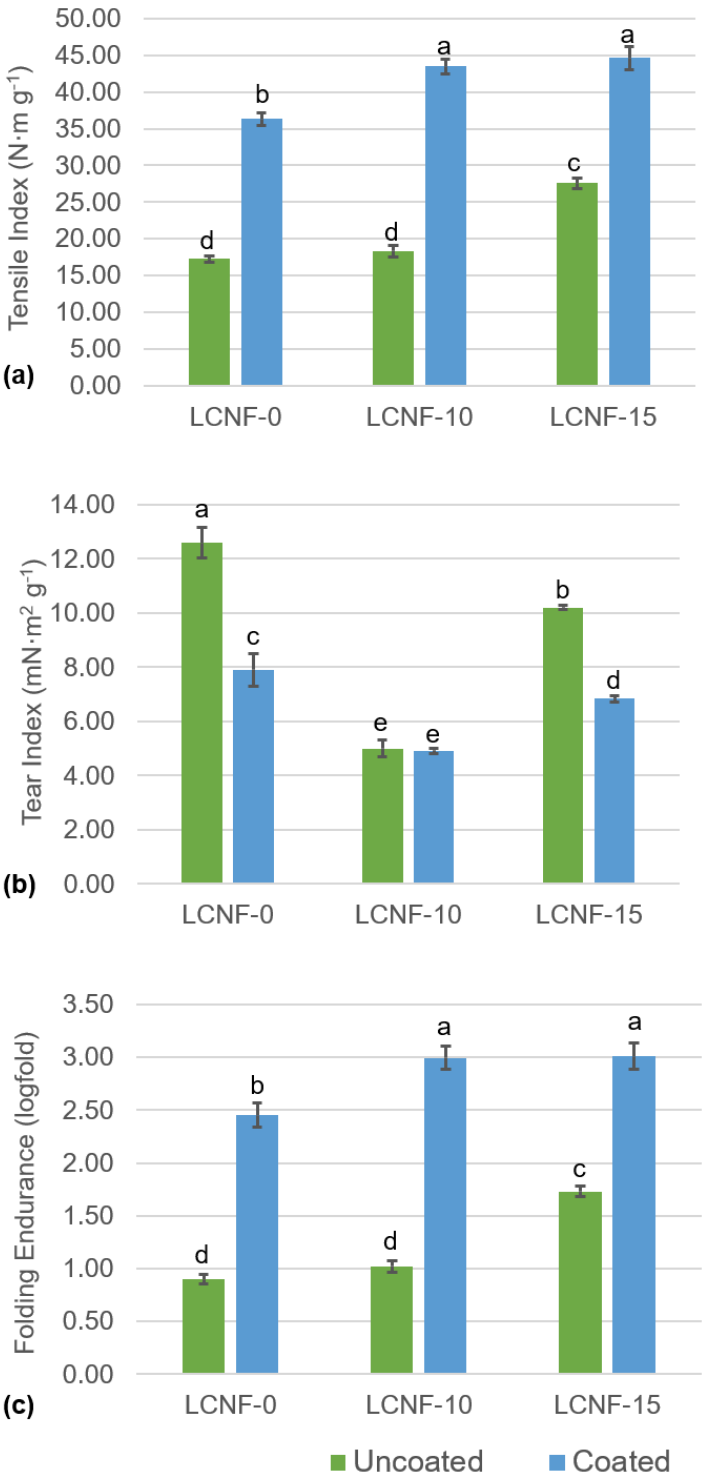


Figure 6

Mechanical properties of uncoated and coated handsheets with 0, 10, and 15% LCNF loading: (a) tensile index; (b) tear index, and (c) folding endurance. Note: Columns with common letters are not significantly different (Tukey's HSD test, $p \leq 0.05$)

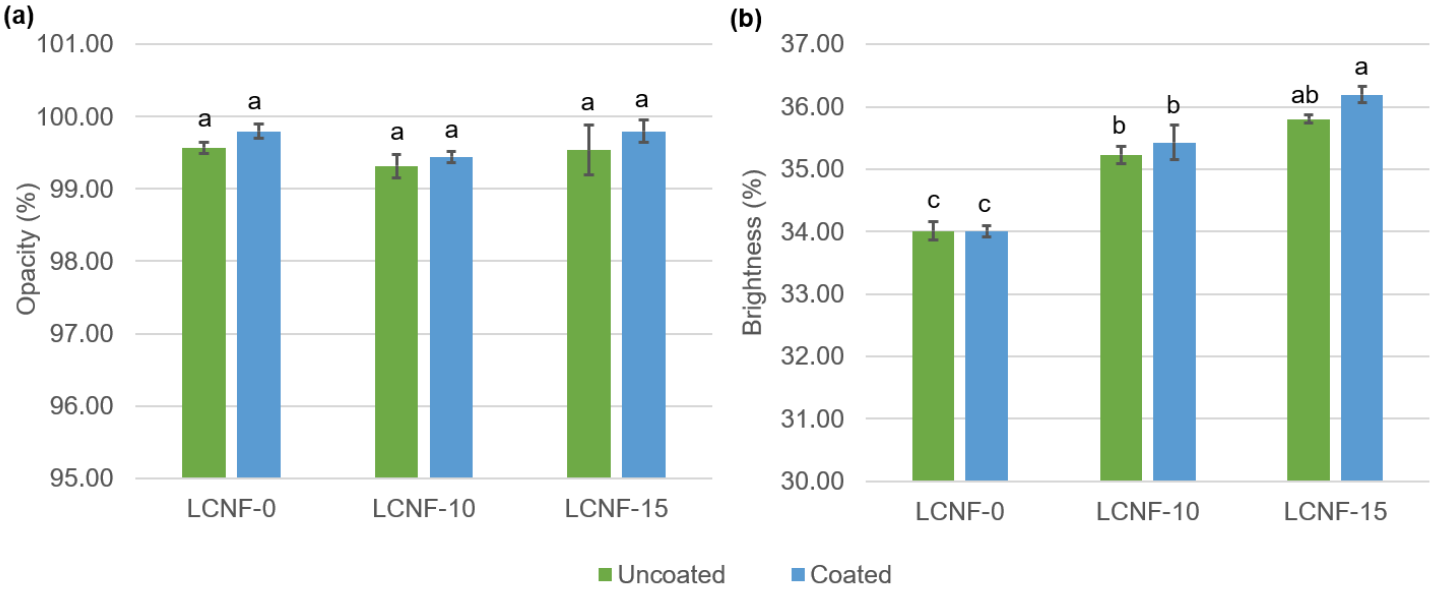


Figure 7

Optical properties of uncoated and coated handsheets measured under illuminant/observer C/2: (a) opacity and (b) brightness. Note: Columns with common letters are not significantly different (Tukey's HSD test, $p \leq 0.05$)

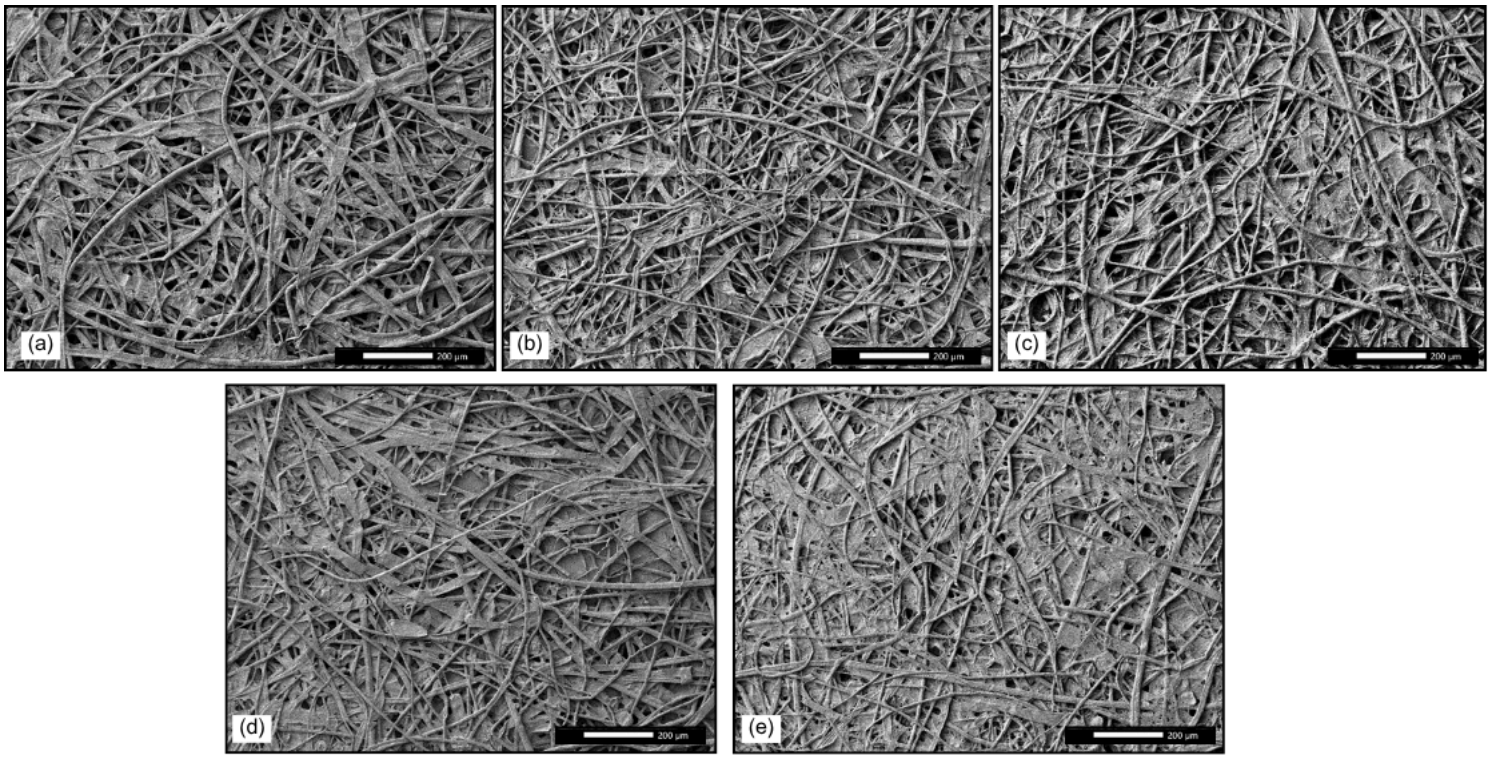


Figure 8

SEM images of representative handsheet samples at 90x magnification: (a) UN-LCNF-0; (b) UN-LCNF-10; (c) UN-LCNF-15; (d) CO-LCNF-0 and (e) CO-LCNF-15. Scale bar = 200 μm.

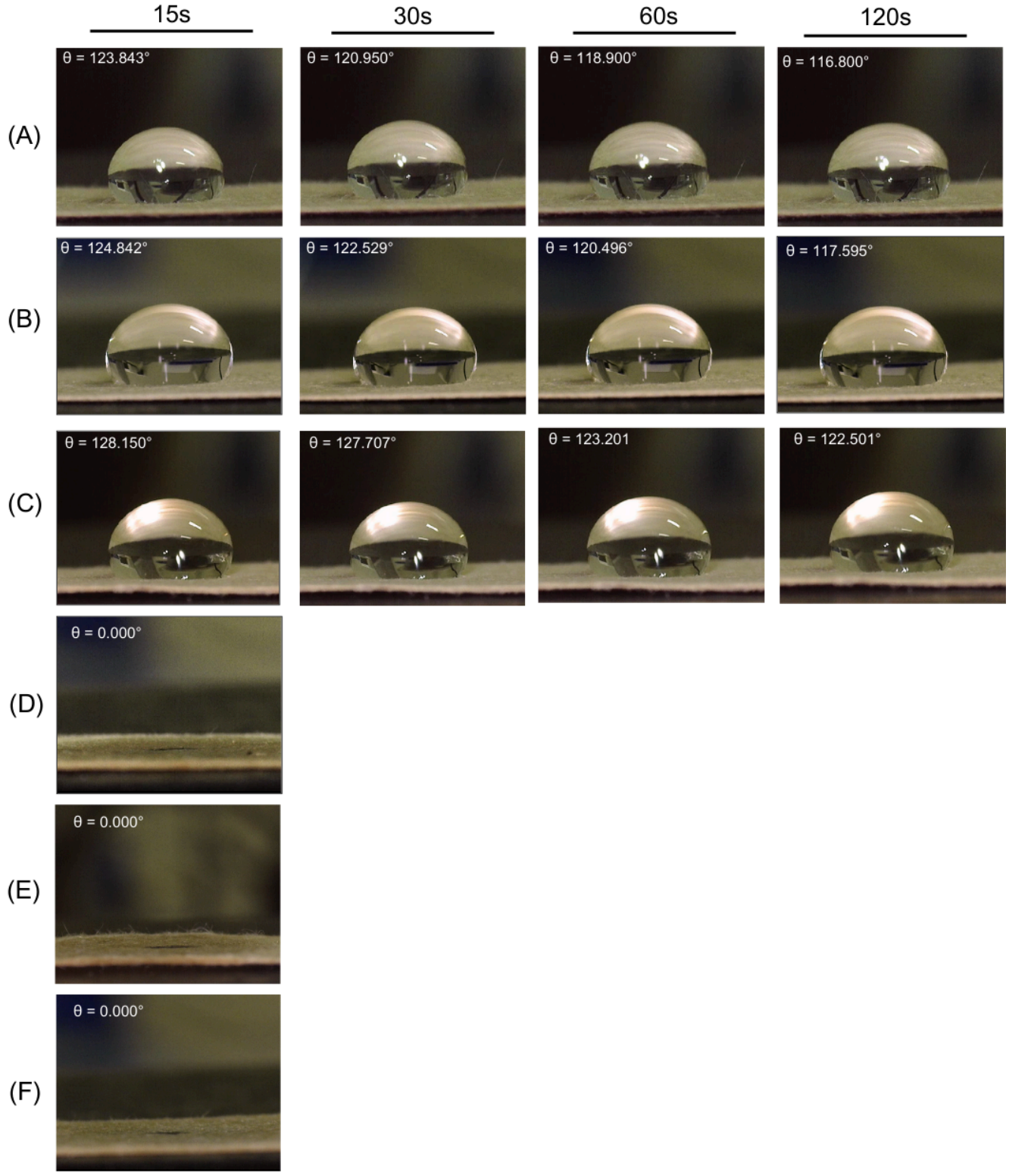


Figure 9

Contact angle measurement of handsheets at 15s, 30s, 60s and 120s holding times: (A) CO-LCNF-0, (B) CO-LCNF-10, (C) CO-LCNF-15, (D) UN-LCNF-0, (E) UN-LCNF-10 and (F) UN-LCNF-15.

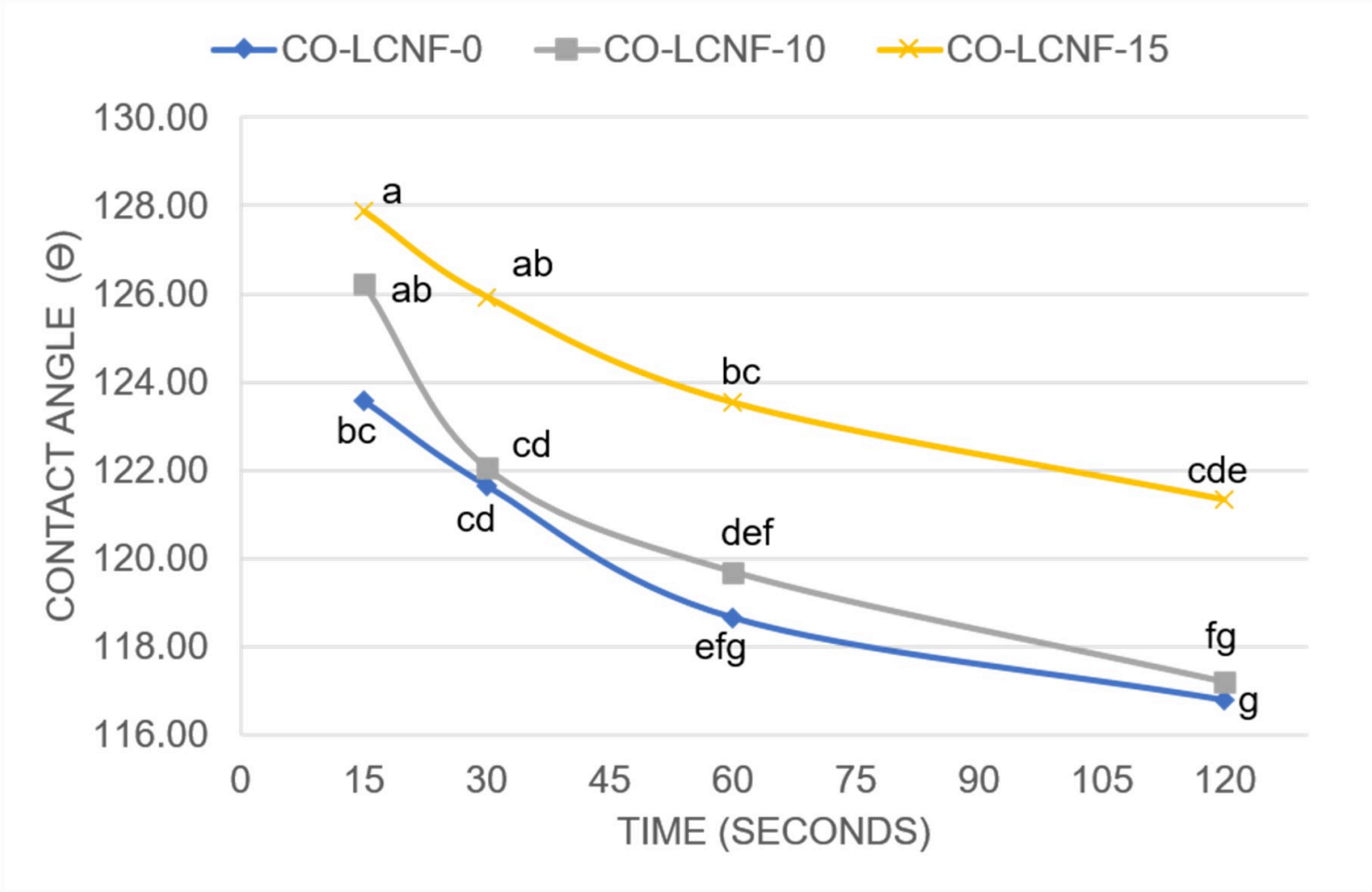


Figure 10

WCA of handsheets as a function of holding time. Note: Plots sharing common letters indicate no significant difference according to Tukey's HSD test at 5% significance level.